Talanta 113 (2013) 135–141

Contents lists available at SciVerse ScienceDirect

Talanta

journal homepage: www.elsevier.com/locate/talanta

Development of a biosensor based on immobilization of acetylcholinesterase on NiO nanoparticles–carboxylic graphene–nafion modified electrode for detection of pesticides

Long Yang, Guangcan Wang*, Yongjun Liu, Min Wang

School of Chemical Science and Engineering, Yunnan University, Kunming 650091, China

ARTICLE INFO

Article history:
Received 16 December 2012
Received in revised form
6 March 2013
Accepted 7 March 2013
Available online 15 March 2013

Keywords:
NiO nanoparticles
Carboxylic graphene
Acetylcholinesterase
Amperometric biosensor
Pesticides

ABSTRACT

A sensitive amperometric acetylcholinesterase (AChE) biosensor based on NiO nanoparticles (NiO NPs), carboxylic graphene (CGR) and nafion (NF) modified glassy carbon electrode (GCE) has been developed. NiO NPs-CGR-NF nanocomposites with excellent conductivity, catalysis and biocompatibility offered an extremely hydrophilic surface for AChE adhesion. The AChE biosensor showed favorable affinity to acetylthiocholine chloride (ATCl) and could catalyze the hydrolysis of ATCl with an apparent Michaelis–Menten constant value of 135 μM. Under optimum conditions, the biosensor detected methyl parathion and chlorpyrifos in the linear range from 1.0×10^{-13} to 1×10^{-10} M and from 1.0×10^{-10} to 1×10^{-8} M with the detection limits 5×10^{-14} M. The biosensor detected carbofuran in the linear range from 1.0×10^{-12} to 1×10^{-10} M and from 1.0×10^{-10} to 1×10^{-8} M with the detection limit of 5×10^{-13} M. The developed biosensor exhibited good sensitivity, stability and reproducibility, thus providing a promising tool for analysis of enzyme inhibitors.

1. Introduction

Over the last decade, biosensors based on AChE have emerged as a promising technique for toxicity analysis, environmental monitoring, food quality control and military investigations [1,2]. The main application of AChE biosensors is for the detection of organophosphate and carbamate pesticides based on enzyme inhibition. These devices are designed to complement or replace the existing reference analytical methods such as chromatographic and coupled chromatographic–spectrometric procedures by simplifying or eliminating sample preparation, thus decreasing the analysis time and cost.

Graphene, a two-dimensional sheet of sp^2-bonded carbon atoms arranged in a honeycomb lattice, has attracted increasing attention since it was first isolated from three-dimensional graphite by mechanical exfoliation [3]. Due to its extraordinary thermal, mechanical, and electrical properties, graphene is usually considered as a competitive candidate for next-generation electronic applications such as electronic and energy storage devices super-capacitors [4,5], batteries [6,7], fuel cells [8,9], solar cells [10,11], sensors [12,13], biosensors [14,15], catalysts [16,17], etc. However, many researches have reported that the pure graphene actually exhibit unsatisfactory electrical conductivity because of the inevitable aggregation [18,19]. Some of the useful and unique properties of graphene can only be realized after it is functionalized with organic groups such as hydroxyl, carboxyl, amino and the like [20,21]. A useful method to prepare functionalized graphene is incorporated into chemical functional groups by covalent bonding on the graphene sheets. Functionalized graphene sheets are easier to disperse in organic solvents, which can improve the dispersion and homogeneity [18,19].

Nanostructured metal oxide semiconductors possess high surface area, nontoxicity, good biocompatibility, catalytic activity and chemical stability. Among the metal oxide semiconductors, nickel oxide (NiO), a p-type semiconductor with a wide band gap of 3.7 eV in room temperature, has been investigated for various applications such as solar cells, lithium-ion batteries, resistive random access memory (RRAM), light-emitting diodes (LEDs), electrochemical sensors and biosensor [22–27]. In recent years, the nanocomposite of NiO NPs and graphene was synthesized and applied in the investigation fields of electrochemistry such as dye sensitized solar cell, lithium-ion batteries, super-capacitors and non-enzymatic glucose sensor [28–32]. However, many of the interesting and unique properties of the nanocomposite can only be realized after it is integrated into more complex assemblies [18,19]. NiO NPs can be separated and formed uniform NiO NPs on functionalized graphene sheets. Based on these existing researches, we developed the AChE biosensor based on NiO NPs-CGR-NF nanocomposite.

* Correspondence to: 2 North Cuihu Road, Kunming 650091,China.
Tel.: +86 871 5033218; fax: +86 871 5153832.
E-mail address: wangc166163@sina.com (G. Wang).

0039-9140/$ - see front matter © 2013 Elsevier B.V. All rights reserved.
http://dx.doi.org/10.1016/j.talanta.2013.03.025

In this work, the CGR and NiO NPs-CGR nanocpmposites have been synthesized by chemical method and characterized by scanning electron microscopy (SEM), fourier transforms infrared spectra (FTIR) and X-ray diffractometer (XRD). The synthesized NiO NPs-CGR nanocomposites are easily dispersed in NF solution. Chitosan (CS) was used to immobilize the AChE on NiO NPs-CGR-NF modified GCE. NF was used as a protective membrane of the AChE biosensors. The NF/AChE-CS/NiO NPs-CGR-NF/GCE biosensor might be an effective device for detection of pesticides.

2. Experimental

2.1. Chemicals

ATCl, AChE (Type C3389, 500 U/mg from electric eel), CS (85% deacetylation), NF (5% in lower aliphatic alcohols and water) were purchased from Sigma-Aldrich (St. Louis, USA). Methyl parathion, chlorpyrifos and carbofuran (99.99%) were obtained from Institution of environmental protection of China's Agriculture Ministry (Beijing China). The graphite powder, bovine serum albumin (BSA) and $Ni(NO_3)_2$ were purchased Shanghai Chemical Reagent Co. Ltd. (China). All other reagents were of analytical grade. Aqueous solutions were prepared with deionized (DI) water (18 MΩ/cm).

2.2. Preparation of CGR

Graphite oxide prepared by Hummer's method [33] was suspended in water and exfoliated through ultrasonication (2 h) to obtain graphene oxide (GO) solution. GO solution was centrifuged at 3000 rpm to remove unexfoliated graphite oxide. CGR was prepared by a chemical method. Briefly, GO aqueous suspension (5 ml) was diluted as to give a concentration of 2.0 mg/ml, and then sonicated for 1 h to give a clear solution. 1.2 g of NaOH and 1.0 g chloroacetic acid (Cl–CH_2–COOH) were added to the suspension and sonicated for 3 h to convert the –OH groups to –COOH via conjugation of acetic acid moieties. Sequentially the suspension was separated by centrifuging at a speed of 15,000 rpm, washed with DI water for several cycles, dried in an oven at 60 °C to gain CGR [34].

2.3. Preparation of NiO NPs-CGR nanocomposites

NiO NPs-CGR nanocomposites were prepared as follows: briefly, 2.0 mg CGR were suspended in 100 μl of 0.01 M $Ni(NO_3)_2$ by sonicating for 10 min to disperse CGR equably. Then 100 μl of 0.01 M sodium citrate, 10.0 ml ethanol and 20.0 ml DI water were added to the above suspension. Ice-cold, freshly prepared 120 μl of 0.05 M $NaBH_4$ solution were added to the above mixture while stirring until the color of the solution did not change. After stirring for an additional 10 h, the black suspending liquid was separated by centrifuging at a speed of 12,000 rpm, washed with DI water for several cycles, dried in an oven at 60 °C. Then, Ni NPs were oxidized to NiO NPs by heating at 120 °C in atmosphere. To improve the crystallinity of NiO NPs in CGR, the product was annealed at 300 °C for 2 h.

2.4. Materials characterization

GO, CGR and NiO NPs-CGR were measured by scanning electron microscopy (SEM, QUNT200 USA), by using a 20 kV accelerated voltage. GO and CGR were measured by Fourier transform infrared spectrometry (FTIR, Thermo Fisher SCIENTIFIC Nicolet IS10 USA). CGR and NiO NPs-CGR were measured by X-ray diffractometer (XRD, Rigaku TTRIII, Japan).

2.5. Preparation of AChE biosensor

NF solution (0.125%, W_t/V) was prepared by diluting 5% of the NF with ethanol and DI water (V/V, 1/1). The NiO NPs-CGR (0.5 mg) were added to 1.0 ml of NF solution and sonicated thoroughly until a homogeneous suspension of NiO NPs-CGR-NF was obtained. Similarly 0.5 mg/ml CGR-NF and GO-NF homogeneous suspensions were obtained. The suspensions were stored at 4 °C. The NiO NPs-CGR-NF/GCE was prepared by casting 5 μl of the 0.5 mg/ml NiO NPs-CGR-NF suspension onto the GCE and drying at room temperature. A similar method was used to prepare GO-NF/GCE and CGR-NF/GCE. The enzyme solution was mixed as 0.05U AChE and 0.2% CS (W_t/V, 50 mM acetic acids). The modified electrodes were each coated 4.5 μl of AChE-CS (V/V, 2/1) and dried at 4 °C. The AChE-CS/GO-NF/GCE, AChE-CS/CGR-NF/GCE and AChE-CS/NiO NPs-CGR/GCE biosensors were obtained and washed with 0.1 M PBS to remove the unbound AChE. Finally, three types of biosensor were each covered with 3 μl 0.1% (W_t/V) NF as the protective membrane. Thus, three types of biosensor structure were NF/AChE-CS/GO-NF/GCE, NF/AChE-CS/CGR-NF/GCE and NF/AChE-CS/NiO NPs-CGR/GCE. Similarly, NF/AChE-CS/GCE was produced as a control.

2.6. Analytical procedures

The electrochemical measurements were carried out on an IM6ex electrochemical workstation (Zahner Elektrik Instruments, Germany). A conventional three-electrode system was employed with a saturated calomel electrode (SCE) as the reference electrode, a platinum foil as the counter electrode, and the modified GCE (diameter = 3 mm) as the working electrodes. Cyclic voltammetry (CV) measurements were performed in 0.1 M phosphate buffer solution (PBS, pH 7.4). The typical current-time plot for the biosensor was gained at 0.47 V after the successive addition of ATCl to PBS with stirring. The apparent Michaelis–Menten constant K_m^{app} of the biosensor was calculated from the Line weaver–Burk equation:

$$\frac{1}{i_{ss}} = \left(\frac{K_m^{app}}{i_{\max}}\right) \times \left(\frac{1}{C}\right) + \left(\frac{1}{i_{\max}}\right) \quad (1)$$

where i_{ss} is the steady-state current after the addition of substrate, $i_{\max}$ is the maximum current measured under saturated substrate condition and C is the concentration of the substrate. The K_m^{app} value, which gives an indication of the enzyme substrate kinetics for the biosensor, was determined by analysis of the slope and intercept of the plot of the reciprocals of steady-state current versus ATCl concentration. The obtained NF/AChE-CS/NiO NPs-CGR-NF/GCE was first immersed in pH7.4 PBS solution containing different concentrations of standard pesticide at room temperature (25 ± 1 °C) for 6-min and then transferred to the electrochemical cell of pH7.4 PBS containing 0.5 mM ATCl to study the amperometric response by CV between 0.0 and 1.0 V. The inhibition of pesticide was calculated as follows:

$$\text{inhibition}(\%) = \frac{i_{P,\text{control}} - i_{P,\text{exp}}}{i_{P,\text{control}}} \times 100\% \quad (2)$$

where $i_{p,\text{control}}$ is the peak current of ATCl on NF/AChE-CS/NiO NPs-CGR/GCE, $i_{p,\text{exp}}$ is the amperometric response of ATCl on NF/AChE-CS/NiO NPs-CGR/GCE with pesticide inhibition.

The detection limit (LD) was calculated by using the equation given below [35]:

$$\text{LD} = 3S/b \quad (3)$$

where S is the standard deviation of the blank solution, b is the slope of the analytical curve.

2.7. Preparation and determination of real samples

The apple and cabbage samples were obtained from local market in Kunming City. Briefly, the apple and cabbage were cleaned and mashed to pulp with a blender, then two sorts of 25.0 g pulp were, respectively, mixed with 50 ml acetonitrile and proper amount of 0.1 M NaCl, and the organic phases were collected and evaporated on a steam bath. The final volume was adjusted to 5.0 ml by adding appropriate amount of dichloromethane. Part of the sample solution was transferred to 0.1 M PBS (pH 7.4) for determination. Two water samples (tap water sample and lake water sample) were filtered through a 0.22 μm membrane and the pH was adjusted to 7.4. After simple pretreatment, different concentrations of chlorpyrifos and carbofuran were added to study the recovery under the optimal conditions.

3. Results and discussion

3.1. Characterizations

The SEM image of Fig. 1(a) showed many layers, wavy and crumpled shapes of GO. Fig. 1(b) indicated few layers crumpled sheets of CGR morphology with the thickness of 3 to 4 nm. The general morphology of the NiO NPs-CGR nanocomposites was observed by SEM in Fig. 1(c). It showed that small NiO NPs were uniformly embedded in the curly CGR nanosheets.

Highly ordered graphite has only a couple of Raman-active bands visible in the spectra (Fig. 2A), the in-phase vibration of the graphite lattice (G band) at 1576 cm^{-1} as well as the (weak) disorder band caused by the graphite edges (D band) at approximately 1355 cm^{-1}. GO of Raman-active bands visible in the spectra (Fig. 2A) as universal is observed that higher disorder in graphite leads to a broader G band, as well as to a broad D band of higher relative intensity compared to that of the G band. The G band broadens of GO significantly and displays a shift to higher frequencies 1357 and1601 cm^{-1} (blue-shift), and the D band grows in intensity. CGR of Raman-active bands visible in the spectra (Fig. 2A) shows the G band shifts back to the position of the G band in graphite, which is attributed to a graphitic "self-healing" similar to what was observed from the sharpening of the G peak and the intensity decrease of the D peak in heat-treated graphite [36]. Raman-active bands are visible in the spectra accord with reference literature [37].

In Fig. 2B, the FTIR spectrum of GO (curve *a*) displayed the presence of –OH (3413 cm^{-1}), C=O (1731 cm^{-1}), C=C (1621 cm^{-1}) and C–O (1047 cm^{-1}), ascribed to the stretching vibrations of GO. FTIR results for the CGR were shown in Fig. 2B (curve *b*). The appearance of strong peaks at 3424 and 1727 cm^{-1} confirmed the presence of the carboxylic group.

Fig. 2C showed the X-ray diffraction patterns of CGR and NiO NPs-CGR nanocomposites. X-ray powder diffraction patterns well defined peaks at 37.2, 43.5, and 62.5° (2θ) indicating the formation of the cubic phase of NiO NPs. The broad diffraction peaks of the NiO NPs indicated small crystal size. Furthermore, the characteristic diffraction peak of the CGR confirmed the presence of CGR in the NiO NPs-CGR nanocomposites.

3.2. Electrochemical behavior of the biosensors

CV of ATCl and enzymatic product thiocholine was investigated on four different biosensors as shown in Fig. 3. No amperometric response could be observed at NF/AChE-CS/GCE (curve *a*), NF/AChE-CS/GO-NF/GCE (curve *b*), NF/AChE-CS/CGR-NF/GCE (curve *c*), and NF/AChE-CS/NiO NPs-CGR-NF/GCE (curve *d*) in PBS (pH 7.4). However, when 0.5 mM ATCl was added into the PBS (pH 7.4), an obvious amperometric response was observed at NF/AChE-CS/GCE (curve *e*), NF/AChE-CS/GO-NF/GCE (curve *f*) NF/AChE-CS/CGR-NF/GCE (curve *g*) and NF/AChE-CS/NiO NPs-CGR-NF/GCE (curve *h*). Obviously, these amperometric responses were attributed to the oxidation of thiocholine produced by the hydrolysis of ATCl, which

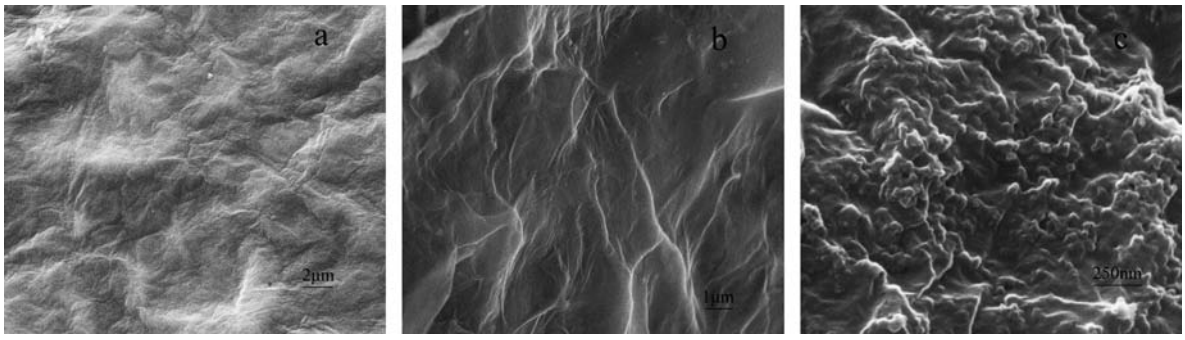

Fig. 1. SEM images of GO (a), CGR (b) and NiO-CGR (c).

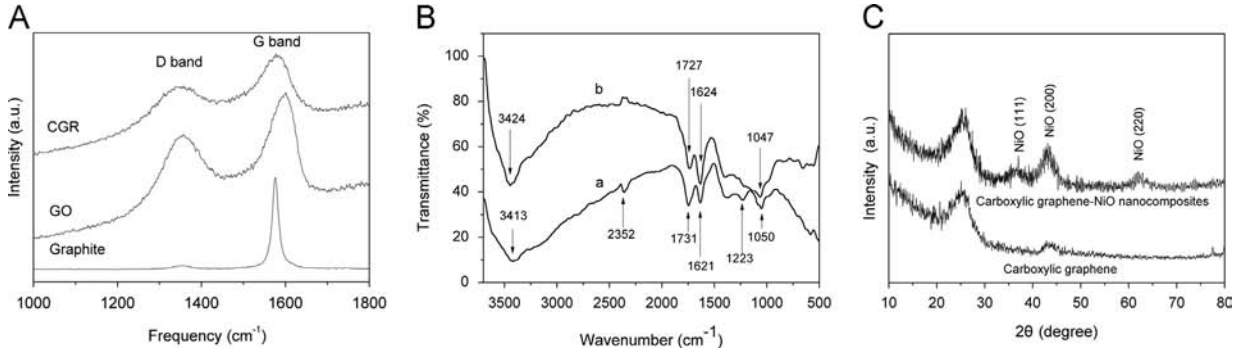

Fig. 2. (A) Raman spectra of graphite, GO and CGR; (B) FTIR spectra of GO (a) and CGR (b); (C) XRD of CGR and NiO-CGR.

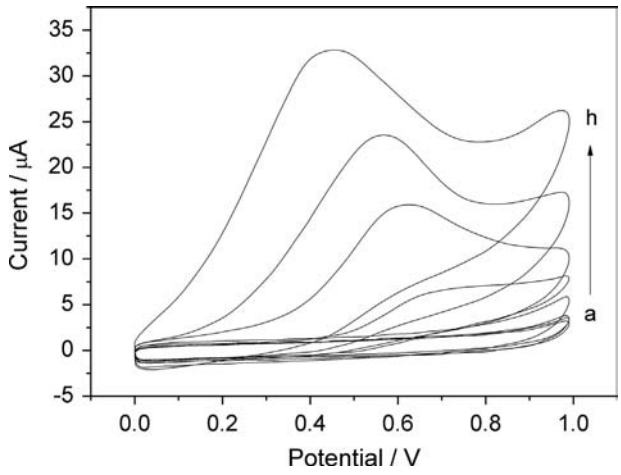

Fig. 3. CV of NF/AChE-CS/GCE (a), NF/AChE-CS/GO-NF/GCE (b), NF/AChE-CS/CGR-NF/GCE (c), NF/AChE-CS/NiO-CGR-NF/GCE (d) in 0.1 M PBS and in 0.1 M PBS containning 0.5 mM ATCl ((e)–(h)), Scan rate: 0.10 V/s in 25 °C.

were catalyzed by immobilized AChE. Fig. 3 showed the oxidation peak currents increased and the oxidation peak potentials shifted to lower potentials in sequence. At NF/AChE-CS/NiO NPs-CGR-NF/GCE, the oxidation peak current was the highest and peak potential was the lowest in four biosensors (curve *h*). It indicated NiO NPs-CGR could greatly improve electron transfer and catalysis which increased peak current and decrease the potential, which was beneficial for avoiding interference from other electroactive species in biological matrix. Obviously, NiO NPs-CGR-NF/GCE with excellent conductivity and catalytic activity provided an extremely hydrophilic surface for AChE adhesion. Besides, NF protective membrane was used to prevent the loss of the enzyme molecules, improve the anti-interference ability of the biosensor and provide a biocompatible microenvironment to maintain enzymatic activity.

3.3. Conductivity, catalysis and biocompatibility of the nanocomposites

In Fig. 3 (curve from *e* to *h*), the oxidation peak currents increased in sequence that indicated the improved conductivity. The oxidation peak potentials shifted to lower potentials orderly that indicated the enhanced catalysis of the nanocomposites.

The biocompatibility was studied by comparing the amperometric response of the NF/AChE-NF/NiO-CGR-NF/GCE (a), NF/AChE-CS/NiO-CGR-NF/GCE (b) and NF/AChE-BSA/NiO-CGR-NF/GCE (c) three biosensors as shown in Fig. S1. The result indicated that the biocompatibility of CS was the best in NF, CS and BSA. Therefore, CS was selected to immobilize AChE that was good for maintaining the high AChE activity.

3.4. Optimization of the preparation of the biosensor

Optimization of volume of NiO NPs-CGR-NF, ratio of NiO NPs in NiO NPs-CGR and amount of immobilized AChE were supplied in Supplementary Materials.

The bioactivity of the immobilized AChE depends on the pH of the ATCl solution. The relationship between amperometric responses of AChE with the pH of the ATCl solution was showed in Fig. S2. In the pH range from 6.8 to 8.0, the amperometric response increased with increasing pH and reached a maximum at 7.4. The further increase the pH of solution led to an obvious decrease of the amperometric response. Therefore, pH 7.4 was used in the detection solution.

In order to enhance the stability of the biosensor, CS was used to immobilize the AChE on NiO NPs-CGR-NF/GCE and to improve electronic transmission between AChE and NiO NPs-CGR-NF/GCE. NF was used as the protective membrane for the AChE biosensor. The NF/AChE-CS/NiONPs-CGR-NF/GCE, AChE-CS/NiONPs-CGR-NF/GCE and AChE/NiONPs-CGR-NF/GCE biosensors were continuously tested 6 times, respectively, in PBS (pH7.4) containing 0.5 mM ATCl solution (Fig. S3). The RSD (7%, curve *b*) of the amperometric response of the AChE-CS/NiONPs-CGR-NF/GCE biosensor was less than the RSD (12%, curve *c*) of the amperometric response of AChE/NiONPs-CGR-NF/GCE biosensor. The RSD (2%, curve *a*) of the amperometric response of NF/AChE-CS/NiONPs-CGR-NF/GCE biosensor was the least in the three biosensors. The results showed that CS and NF effectively improved the stability of the AChE biosensor.

3.5. Detection of ATCl

The AChE biosensor was explored by CV measurements according to the above optimum conditions. Fig. 4A showed the typical current-time plot for the NF/AChE-CS/NiO NPs-CGR/GCE biosensor at 0.47 V on successive addition of stock ATCl to 0.1 M PBS. With increasing ATCl concentration, the amperometric response of the biosensor increased. The amperometric response of the biosensor

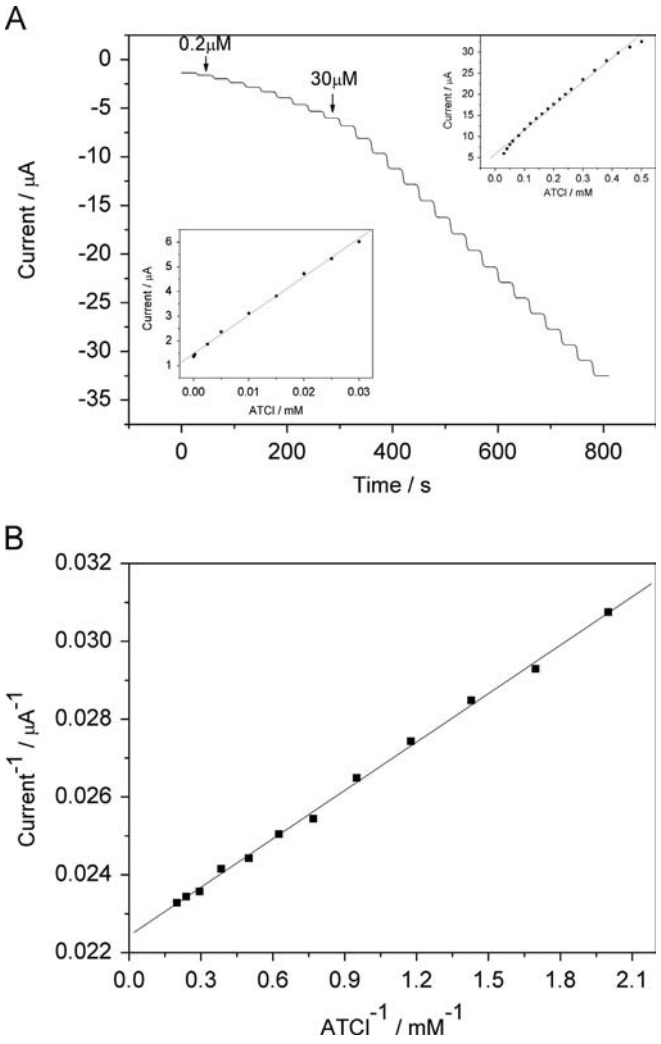

Fig. 4. (A) Typical current-time plot for the sensor on successive addition of stock ATCl to 0.1 M PBS, insets show the calibration curves for ATCl determination; (B) Lineweaver–Burk plot of $1/i_{ss}$ vs. $1/C$.

was a linear function of ATCl concentration in two segments. One was from 0.2 to 30 μM; the other was from 30 to 500 μM. The two linear ranges indicated that the linear range of AChE biosensors for acetylcholine was approximately two orders of magnitude. When the concentration of ATCl was saturated, the amperometric response gradually tended to a constant value. The detection limit was 0.1 μM. At higher ATCl concentrations the shape of the amperometric response was indicative of a Michaelis–Menten process (Fig. 4B). The apparent Michaelis–Menten constant (K_m^{app}) in the present studies was calculated to be 135 μM according to Lineweaver–Burk equation. This value was lower than that for AChE adsorbed on reduced graphene oxide–gold nanocomposites modified electrode (0.16 mM) [38], for AChE immobilized on CdS-decorated graphene nanocomposite modified electrode (0.24 mM) [39] and for AChE adsorbed on liposome bioreactors-chitosan nanocomposite film modified electrode (0.36 mM) [40] indicating that the AChE biosensor had a great affinity and catalysis to its substrate ATCl.

3.6. Effect of incubation time

The activity of the AChE was influenced by the incubation time of the AChE to Pesticides. The inhibition level of AChE increased with increasing incubation time (Fig. S4). Considering the whole analytical time and sensitivity of the amperometric measurements, 6-min exposure time was chosen as the best compromise between signal and exposure time.

3.7. Pesticides detection

The inhibition of pesticide led to the decrease of the activity and biological functions of AChE. Therefore, detecting the amperometric response from thiocholine on the biosensor was a simple and effective way to biomonitoring pesticide exposure. As shown in Fig. 5A, after incubation of NF/AChE-CS/NiO NPs-CGR-NF/GCE with 10^{-12} M methyl parathion for 6-min, the amperometric response (curve *b*) decreased comparing with the intact AChE (curve *a*). After incubation of NF/AChE-CS/NiO NPs-CGR-NF/GCE with 10^{-8} M methyl parathion for 6-min, the amperometric response (curve *c*) greatly decreased comparing with the intact AChE (curve *a*). Inhibition effects were investigated by measuring the biosensor response towards 0.5 mM ATCl after inhibited by different concentrations of methyl parathion, chlorpyrifos and carbofuran, respectively. The calibration plots of inhibition percentage versus pesticides concentration were showed in Fig. 5B. Linear relationships between inhibition percentage and the concentration of pesticides were showed in Table S1. The two linear ranges indicated that the biosensor was more sensitive for detecting low concentration of pesticides than high concentration of pesticides. The performances of the biosensor were compared with other AChE biosensors reported by literatures (Table 1).

Inhibition effects were also investigated by DPV. As shown in Fig. S5, the response of the biosensor before and after 6 min incubation in 10^{-12}, 10^{-11}, 10^{-10}, 10^{-9} and 10^{-8} M carbofuran, the peak currents (curves *b–f*) dramatically decreased compared with that on the control (curve *a*), and the decrease in peak current increased with the increasing concentration of carbofuran. The calibration plot of inhibition percentage versus carbofuran concentration was showed in Fig. S6. Linear equations of carbofuran were I(%)=12.61lgC+174.90 (r=0.998) from 10^{-12} to 10^{-10} M and I(%)=5.35lgC+101.87 (r=0.997) from 10^{-10} to 10^{-8} M with the detection limit of 5.0×10^{-13} M. The result indicated that DPV analysis had high resolution and sensitivity than CV.

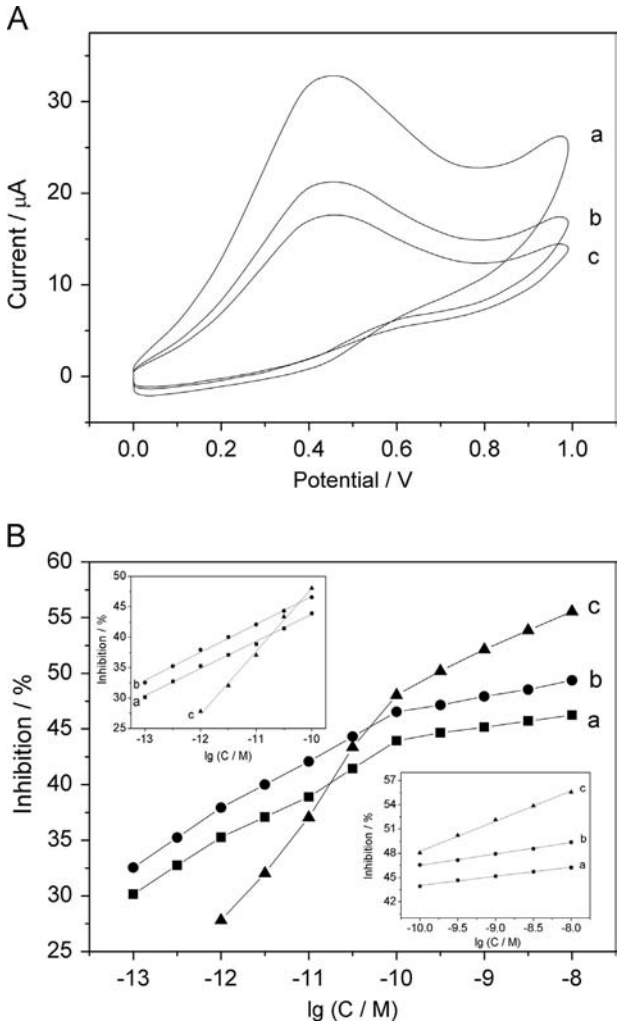

Fig. 5. (A) CV of the NF/AChE-CS/NiO-CGR-NF/GCE in 0.1 M PBS containing 0.5 mM ATCl after incubation with 0 (a), 10^{-12} M (b) and 10^{-8} M (c) methyl parathion for 6-min; (B) Inhibition curves of NF/AChE-CS/NiO-CGR-NF/GCE biosensor for methyl parathion (a) and chlorpyrifos (b) and carbofuran (c) determination by CV.

3.8. Interference study

The interfering signal due to the most common electroactive species was studied. The signal for a 0.5 mM ATCl was compared with the signal obtained in the presence of the interfering species. The test result showed no noticeable changes in amperometric response were detected in the presence of glucose (0.5 mM), citric acid (0.5 mM), oxalic acid (0.5 mM), PO_4^{3-} (0.5 mM), SO_4^{2-} (0.5 mM), NO_3^- (0.5 mM), Cu(II) (0.5 mM) and Pb(II) (0.5 mM), respectively, at the present operating potential in this system. However, 0.5 mM of *p*-nitrophenol, 0.5 mM of nitrobenzene, 0.5 mM of *p*-nitroaniline, 0.5 mM of trinitrotoluene, 0.5 mM of toluene and 0.5 mM of *p*-toluenesulfonic acid severely interfered with the determination. Besides, equal concentration of methyl parathion, chlorpyrifos and carbofuran severely interfered with each other for the determination. The interference study results were showed in Fig. S7.

3.9. Precision of measurements and stability of biosensor

The intra-assay precision of the biosensor was evaluated by testing one NF/AChE-CS/NiO NPs-CGR-NF/GCE for six times in 0.5 mM ATCl after being immersed in the 1.0×10^{-10} M methyl parathion for 6-min. The inter-assay precision was estimated with

Table 1
Comparisons of the response of the biosensor for detection of pesticides with other biosensor based on AChE.

Sample	Electrode	Liner range (M)	Detection limit (M)	References
Methyl parathion	AChE-LDHs[a]/GCE	1.9×10^{-8}–1.1×10^{-6}; 1.1×10^{-6}–1.5×10^{-5}	2.3×10^{-9}	[41]
	AChE-SF[b]/MWNTs[c]/GCE	3.5×10^{-6}–2.0×10^{-3}	5.0×10^{-7}	[42]
	NF/AChE-CS/NiO-CGR-NF/GCE	10^{-13}–10^{-10}; 10^{-10}–10^{-8}	5.0×10^{-14}	This work
Chlorpyrifos	AChE/CPBA[d]/GR[e]-AuNPs/GCE	1.4×10^{-9}–2.9×10^{-8}; 2.9×10^{-8}–2.9×10^{-7}	2.9×10^{-10}	[38]
	PATP[f] membranes/AuNPs	5.0×10^{-7}–1.0×10^{-5}	3.3×10^{-7}	[43]
	NF/AChE-CS/NiO-CGR-NF/GCE	10^{-12}–10^{-10}; 10^{-10}–10^{-8}	5.0×10^{-13}	This work
Carbofuran	AChE/PAMAM[g]-Au/CNTs/GCE	4.5×10^{-9}–9.0×10^{-8}	4.0×10^{-9}	[44]
	AChE-TCNQ[h]/SPE[i]	9.0×10^{-10}–7.5×10^{-7}	9.0×10^{-10}	[45]
	NF/AChE-CS/NiO-CGR-NF/GCE	10^{-12}–10^{-10}; 10^{-10}–10^{-8}	5.0×10^{-13}	This work

[a] Layered double hydroxides.
[b] Silk fibroin.
[c] Multiwalled carbon nanotube.
[d] 3-Carboxyphenylboronic acid.
[e] Graphene.
[f] Polyaminothiophenol.
[g] Polyamidoamine.
[h] 7,7,8,8-Tetracyanoquinodimethane.
[i] Screen-printed electrode.

six different biosensors in the same way. The two RSD of intra-assay and inter-assay were found to be 3.4 and 6.5%, respectively, indicating an acceptable reproducibility. When the enzyme electrode was not in use, it was stored at 4 °C in dry condition. No obvious decrease in the response of ATCl was observed in the first 10-day storage. After a 30-day storage period, the sensor retained 91% of its initial amperometric response, indicating the acceptable stability of biosensor.

3.10. Analytical real samples

To investigate the accuracy of an analytical method, spike recovery is a useful tool. The variability was low if there were no interferences or matrix effects, so a recovery close to 100% was expected. Table S2 showed the results obtained by analysis of these spiked samples. The recoveries of apple, cabbage, tap water and lake water samples were observed in the ran ge of 93.0–105.2%, which demonstrated low matrix effect on the amperometric response. The low relative standard deviations for chlorpyrifos and carbofuran demonstrated the high precision of analysis.

4. Conclusion

In this paper, combining the advantageous characteristics of CGR, NiO NPs and NF, the NiO NPs-CGR-NF nanocomposites have been prepared. The NiO NPs-CGR-NF nanocomposites with excellent conductivity, catalysis and biocompatibility offered an extremely hydrophilic surface that was favorable for AChE adhesion, biological activity maintenance and conductivity between AChE and modified electrode. CS was used as to immobilize the AChE on NiO NPs-CGR-NF/GCE. NF was used as the protective membrane of the AChE biosensor to improve stability. The NF/AChE-CS/NiO NPs-CGR-NF biosensor has been developed. The constructed biosensor exhibited many advantages such as low applied potential, good fabrication reproducibility, acceptable stability, fast response and low detection limit. The biosensor has potential application in biomonitoring of methyl parathion, chlorpyrifos and carbofuran pesticides and other organophosphate and carbamate pesticides. The method not only can be used to immobilize other enzymes to construct a range of biosensors but also may be extended to assemble other biological molecules, such as antibody, antigen and DNA for wide bioassay applications.

Appendix A. Supporting information

Supplementary data associated with this article can be found in the online version at http://dx.doi.org/10.1016/j.talanta.2013.03.025.

References

[1] N.A. Hosea, H.A. Berman, P. Taylor, Biochemistry 34 (1995) 11528–11536.
[2] S. Andreescu, J.L. Marty, Biomol. Eng. 23 (2006) 1–15.
[3] K.S. Novoselov, A.K. Geim, S.V. Morozov, D. Jiang, Y. Zhang, S.V. Dubonos, I. V. Grigorieva, A.A. Firsov, Science 306 (2004) 666–669.
[4] M.D. Stoller, S.J. Park, Y.W. Zhu, J.H. An, R.S. Ruoff, Nano Lett. 8 (2008) 3498–3502.
[5] A.K. Mishra, S. Ramaprabhu, J. Phys. Chem. C 115 (2011) 14006–14013.
[6] E. Yoo, J. Kim, E. Hosono, H.S. Zhou, T. Kudo, I. Honma, Nano Lett. 8 (2008) 2277–2282.
[7] J. Xiao, D. Mei, X. Li, W. Xu, D. Wang, G.L. Graff, W.D. Bennett, Z. Nie, L.V. Saraf, I.A. Aksay, J. Liu, J.G. Zhang, Nano Lett. 11 (2011) 5071–5078.
[8] B. Seger, P.V. Kamat, J. Phys. Chem. C 113 (2009) 7990–7995.
[9] R. Kou, Y.Y. Shao, D.H. Wang, M.H. Engelhard, J.H. Kwak, J. Wang, V. V. Viswanathan, C.M. Wang, Y.H. Lin, Y. Wang, I.A. Aksay, J. Liu, Electrochem. Commun. 11 (2009) 954–957.
[10] X. Wang, L.J. Zhi, N. Tsao, Z. Tomovic, J.L. Li, K. Mullen, Angew. Chem. Int. Ed. 47 (2008) 2990–2992.
[11] J.B. Wu, H.A. Becerril, Z.N. Bao, Z.F. Liu, Y.S. Chen, P. Peumans, Appl. Phys. Lett. 92 (2008) 263302–263303.
[12] S.J. Guo, S.J. Dong, J. Mater. Chem. 21 (2011) 18503–18516.
[13] X.Y. Yang, X.Y. Zhang, Y.F. Ma, Y. Huang, Y.S. Wang, Y.S. Chen, J. Mater. Chem. 19 (2009) 2710–2714.
[14] Y. Wang, S. Zhang, D. Du, Y.Y. Shao, Z.H. Li, J. Wang, M.H. Engelhard, J.H. Li, Y. H. Lin, J. Mater. Chem. 21 (2011) 5319–5325.
[15] J.D. Qiu, J. Huang, R.P. Liang, Sens. Actuators, B 160 (2011) 287–294.
[16] S.S. Han, H. Kim, N. Park, J. Phys. Chem. C 115 (2011) 24696–24701.
[17] R.F. Nie, J.H. Wang, L.N. Wang, Y. Qin, P. Chen, Z.Y. Hou, Carbon 50 (2012) 586–596.
[18] S. Stankovich, D.A. Dikin, G.H.B. Dommett, K.M. Kohlhaas, E.J. Zimney, E. A. Stach, R.D. Piner, S.T. Nguyen, R.S. Ruoff, Nature 442 (2006) 282–286.
[19] D. Li, R.B. Kaner, Science 320 (2008) 1170–1171.
[20] Q.L. Sheng, M.Z. Wang, J.B. Zheng, Sens. Actuators. B 160 (2011) 1070–1077.
[21] D. Zheng, S.K. Vashist, K. Al-Rubeaan, J.H.T. Luong, F.S. Sheu, Talanta 99 (2012) 22–28.
[22] Z.J. Huang, G. Natu, Z.Q. Ji, P. Hasin, Y.Y. Wu, J. Phys. Chem. C 115 (2011) 25109–25114.
[23] Y.N. Nuli, S.L. Zhao, Q.Z. Qin, J. Power Sources 114 (2003) 113–120.
[24] F. Li, H.Y. Chen, C.M. Wang, K.A. Hu, J. Electroanal. Chem. 531 (2002) 53–60.
[25] R. Waser, R. Dittmann, G. Staikov, K. Szot, Adv. Mater. 21 (2009) 2632–2663.
[26] J.M. Caruge, J.E. Halpert, V. Bulovic, M.G. Bawendi, Nano Lett. 6 (2006) 2991–2994.
[27] X.F. Song, L. Gao, S. Mathur, J. Phys. Chem. C 115 (2011) 21730–21735.
[28] H.B. Yang, G.H. Guai, C.X. Guo, Q.L. Song, S.P. Jiang, Y.L. Wang, W. Zhang, C. M. Li, J. Phys. Chem. C 115 (2011) 12209–12215.
[29] M. Latorre-Sanchez, P. Atienzar, G. Abellán, M. Puche, V. Fornés, A. Ribera, H. García, Carbon 50 (2012) 518–525.

[30] D.L. Fang, Z.D. Chen, X. Liu, Z.F. Wu, C.H. Zheng, Electrochim. Acta 81 (2012) 321–329.
[31] W. Lva, F.M. Jin, Q.G. Guo, Q.H. Yang, F.Y. Kang, Electrochim. Acta 73 (2012) 129–135.
[32] Y.Q. Zhang, Y.Z. Wang, J.B. Jia, J.G. Wang, Sens. Actuators, B 171–172 (2012) 580–587.
[33] W.S. Hummers, R.E. Offeman, J. Am. Chem. Soc. 80 (1958) 1339–1339.
[34] X.M. Sun, Z. Liu, K. Welsher, J.T. Robinson, A. Goodwin, S. Zaric, H.J. Dai, Nano Res. 1 (2008) 203–212.
[35] I. Krull, M. Swartz, LC–GC 16 (1998) 922–924.
[36] K. Sato, R. Saito, Y. Oyama, et al., Chem. Phy. Lett. 427 (2006) 117–121.
[37] K.N. Kudin, B. Ozbas, H.C. Schniepp, R.K. Prud'homme, I.A. Aksay, R. Car, Nano Lett. 8 (2008) 36–41.
[38] T. Liu, H.C. Su, X.J. Qu, P. Ju, L. Cui, S.S. Ai, Sens. Actuators, B 160 (2011) 1255–1261.
[39] K. Wang, Q. Liu, L.n. Dai, J.J. Yan, C. Ju, B.J. Qiu, X.Y. Wu, Anal. Chim. Acta 695 (2011) 84–88.
[40] H.N. Guan, F.L. Zhang, J. Yu, D.F. Chi, Food Res. Int. 49 (2012) 15–21.
[41] J.M. Gong, Z.Q. Guan, D.D. Song, Biosens. Bioelectron. 39 (2013) 320–323.
[42] R. Xue, T.F. Kang, L.P. Lu, S.Y. Cheng, Appl. Surf. Sci. 258 (2012) 6040–6045.
[43] C.G. Xie, H.F. Li, S.Q. Li, J. Wu, Z.P. Zhang, Anal. Chem. 82 (2010) 241–249.
[44] Y.H. Qu, Q. Sun, F. Xiao, G.Y. Shi, L.T. Jin, Bioelectrochemistry 77 (2010) 139–144.
[45] G. Silva Nunes, G. Jeanty, J.L. Marty, Anal. Chim. Acta 523 (2004) 107–115.